

Formation of syngenetic and early diagenetic iron minerals in the late Archean Mt. McRae Shale, Hamersley Basin, Australia: New insights on the patterns, controls and paleoenvironmental implications of authigenic mineral formation

Rob Raiswell^{a,*}, Christopher T. Reinhard^b, Arkadiusz Derkowski^c, Jeremy Owens^b, Simon H. Bottrell^a, Ariel D. Anbar^d, Timothy W. Lyons^b

^a School of Earth and Environment, University of Leeds, Leeds LS2 9JT, UK

^b Department of Earth Sciences, University of California, Riverside, CA 92521, USA

^c Institute of Geological Sciences, Polish Academy of Sciences, Senacka 1, Krakow 31-002, Poland

^d School of Earth and Space Exploration and Department of Chemistry and Biochemistry, Arizona State University, Tempe, AZ 85287, USA

Received 17 May 2010; accepted in revised form 12 November 2010; available online 19 November 2010

Abstract

A section through the late Archean Mt. McRae Shale comprising, in ascending order, a lower shale interval (LSI), a banded iron formation (BIF), an upper shale (USI) and a carbonate (C1) has been analyzed for total Fe and Al contents and authigenic Fe present as carbonate, oxide, sulfide and silicate phases. The authigenic mineralogy is controlled by the episodic addition of Fe from hydrothermal activity and removal of Fe by sulfide, relative to rates of clastic sedimentation. The LSI and BIF have mean Fe_T/Al values of 2 and 5, respectively, that record iron enrichment from hydrothermal sources. Iron was precipitated primarily as siderite accompanied by Fe-rich chlorite from anoxic bottom waters rich in dissolved Fe. Pyrite formation was probably limited by the availability of sulfate, which was present at low concentrations and became rapidly depleted. The USI has generally lower Fe_T/Al values (0.6–1.3), similar to those found in Paleozoic shales, with the exception of one interval where enrichment may reflect either a weak hydrothermal source or the operation of an iron shuttle. This interval contains authigenic Fe predominantly as pyrite, where high values for DOP (>0.8) indicate the existence of a water column that became rich in dissolved sulfide (euxinic) when sulfate concentrations increased due to a transient or secular increase in ocean/atmosphere oxygenation. High concentrations of dissolved sulfide maintained low concentrations of dissolved Fe, which allowed only minor amounts of Fe to be precipitated as carbonates and silicates. The USI also has elevated concentrations of organic matter that most probably reflect increased productivity and likely limited euxinia to midportions of the water column on the basin margin. The carbonate C1 represents a basinal chemistry where sulfide has been removed and Fe_T/Al values are ~ 1 indicating that hydrothermal activity again produced dissolved Fe-rich bottom waters. Detailed iron speciation of the Mt. McRae Shale can be used to recognize spatial and temporal variations in iron and sulfur inputs to the late Archean Hamersley Basin, just prior to the Paleoproterozoic rise in atmospheric oxygenation, and our refined methods have relevance to all Fe-rich deposits.

© 2010 Elsevier Ltd. All rights reserved.

1. INTRODUCTION

Paleoproterozoic rocks record evidence for a rapid rise in atmospheric O_2 (termed the Great Oxidation Event or GOE; see Holland, 1962, 1992, 2002; Karhu and Holland,

* Corresponding author. Tel.: +44 1133 435200.

E-mail address: r.raiswell@see.leeds.ac.uk (R. Raiswell).

1994; Bekker et al., 2004; Canfield, 2005) between 2.45 and 2.32 Ga (1 Ga = 10^9 years), which enhanced oxidative weathering of pyrite on land and increased sulfate concentrations in the ocean (Canfield et al., 2000). Sulfate addition in turn stimulated biogenic sulfate reduction, leading to syngenetic pyrite in the water column and diagenetic pyrite formation in the sediments. More recently, detailed chemostratigraphy of the Mt. McRae Shale (Hamersley Group, Western Australia) deposited at ~ 2.5 Ga in the late Archean (perhaps 100 million years prior to the GOE) has shown evidence for an earlier introduction of oxygen recognized by non-mass-dependent sulfur isotope behavior (Kaufman et al., 2007) and by localized enrichments of redox sensitive transition elements (Mo and Re; Anbar et al., 2007). This oxygenation event also stimulated a surface oxidative cycle, which increased concentrations of seawater sulfate and enabled sulfate reduction to produce an H_2S -bearing water column (Reinhard et al., 2009). The addition of H_2S removed dissolved Fe^{2+} from the water column and produced pyritic sediments with C–S–Fe signatures characteristic of H_2S -bearing, euxinic bottom waters.

During the late Archean oxygenic photosynthesis occurred where nutrient levels were sufficiently high, such as in surface waters along continental margins (Kendall et al., 2010). The atmospheric evolution resulting from primary productivity was not the single external driver of basin seawater composition during the deposition of the Mt. McRae Shale, however, as there were also significant (and probably varying) inputs of dissolved iron by hydrothermal activity (Morris and Horowitz, 1983; Klein and Beukes, 1989; Derry and Jacobsen, 1990; Bau and Moller, 1993; Ohmoto et al., 2006). Here we show how the relationship between additions of seawater sulfate (by oxidative weathering) and dissolved iron (by hydrothermal activity) controlled the formation of authigenic iron carbonate, sulfide and silicate minerals in the Mt. McRae Shale. A reducing Archean ocean, near-saturation with respect to calcite and amorphous silica, produced mineralogical variations in pyrite, iron-rich/iron-depleted carbonates and silicates as a result of the interplay between episodic addition of iron sourced by hydrothermal activity, sulfide sourced by sulfate reduction and rates of clastic sedimentation. Shales produced by relatively high rates of clastic sedimentation are linked to low rates of authigenic iron accumulation that may reflect limited time available for syngenetic and early diagenetic iron mineral formation and accumulation. Here, for the first time, we combine quantitative XRD with standard methods of Fe speciation specially adapted and refined for the full range of iron minerals expected under the dynamic paleoceanographic conditions at the dawn of biospheric oxygenation. The general approach, and specific refinements described here, are broadly relevant to studies of paleoredox conditions in rocks of all ages, particularly those deposited from Fe-rich waters.

2. GEOLOGY AND PETROLOGY

Core ABDP-9 was drilled during 2004 as part of the Astrobiology Drilling Program of the NASA Astrobiology Institute. The purpose of this drilling program was to ob-

tain samples free from modern contamination and weathering effects for biogeochemical analysis. The drill site was located at $21^{\circ}59'29.5''S$, $117^{\circ}25'13.6''E$ on the Pilbara craton of Western Australia and comprises approximately 1000 m of banded iron formation, kerogenous shales, basinal carbonates, cherts and clastics in the lower part of the Hamersley Group. The base of the core is the Mt. Sylvia Formation, which passes up into 85 m of Mt. McRae Shale and is capped by the Dales Gorge Member of the Brockman Iron Formation. These sediments have experienced only mild metamorphism (prehnite–pumpellyite facies to $<300^{\circ}C$) and minimal deformation (Anbar et al., 2007; Kaufman et al., 2007). The core was sampled at 0.2–2 m intervals.

The Mt. McRae Shale in core ABDP-9 (Fig. 1) consists of four main units (Anbar et al., 2007; Kaufman et al., 2007). The base of the sequence (189.65–173 m) is a lower shale interval (LSI), which comprises interbedded organic-rich marl and laminated shale. Above this (to 153.3 m) is mainly sideritic BIF with one marl near the base and a package of thin laminated shales toward the top. Another shale (the upper shale interval or USI) occurs above the BIF up to 125.5 m depth and comprises mainly black laminated shale. Pyrite nodules occur between 131 and 134 m and pyritic laminae from 134 to 143 m. Both the USI and LSI contain several weight percent (wt%) pyrite S and typically >3 wt% organic C. A carbonate (125.5–118.5 m) occurs above the USI and is here termed C1. The shales have been enriched in iron (Reinhard et al., 2009) but otherwise have compositions that are typical of terrigenous muds (Alibert and McCulloch, 1993). These finely laminated sediments are thought to be hemipelagites deposited in an outer-shelf or slope environment and may be distal turbidites (Krapez et al., 2003). The BIF represents a more extreme iron enrichment (Reinhard et al., 2009) but the precursor sediments were probably essentially the same deep-water muds. The carbonate is well laminated and deposition must have occurred below wave-base, indicating a pelagic origin. Original textures have otherwise been largely destroyed by diagenetic recrystallization (Krapez et al., 2003).

Mineralogical data for the Mt. McRae Shale are sparse compared to the overlying Dales Gorge Member. These data are summarized here as reported in the literature, although later we adopt current nomenclature for iron silicates (see Brigattii et al., 2006) in which chamosite is termed Fe-rich chlorite, greenalite is Fe-rich serpentine, stilpnomelane is Fe-rich mica and minnesotaite is Fe-rich talc. The Dales Gorge Member typically comprises two mineral assemblages: a hematite–magnetite–chert assemblage (BIF) and a chert–silicate–carbonate assemblage associated with shale. Both assemblages contain Fe-rich syngenetic or early diagenetic minerals, but the hematite–magnetite–chert assemblage has a low proportion of clastics, in contrast to the chert–silicate–carbonate facies, which was deposited in association with a distal source of clastics (possibly volcanic ash). The black shale mineralogy in the Dales Gorge BIF is highly variable but the main minerals are reported to be chert, siderite, dolomite, ankerite/ferroan dolomite, quartz, mica, K-feldspar, minnesotaite, clinochlore and greenalite (Trendall and Blockley, 1970; Ewers and Morris, 1981;

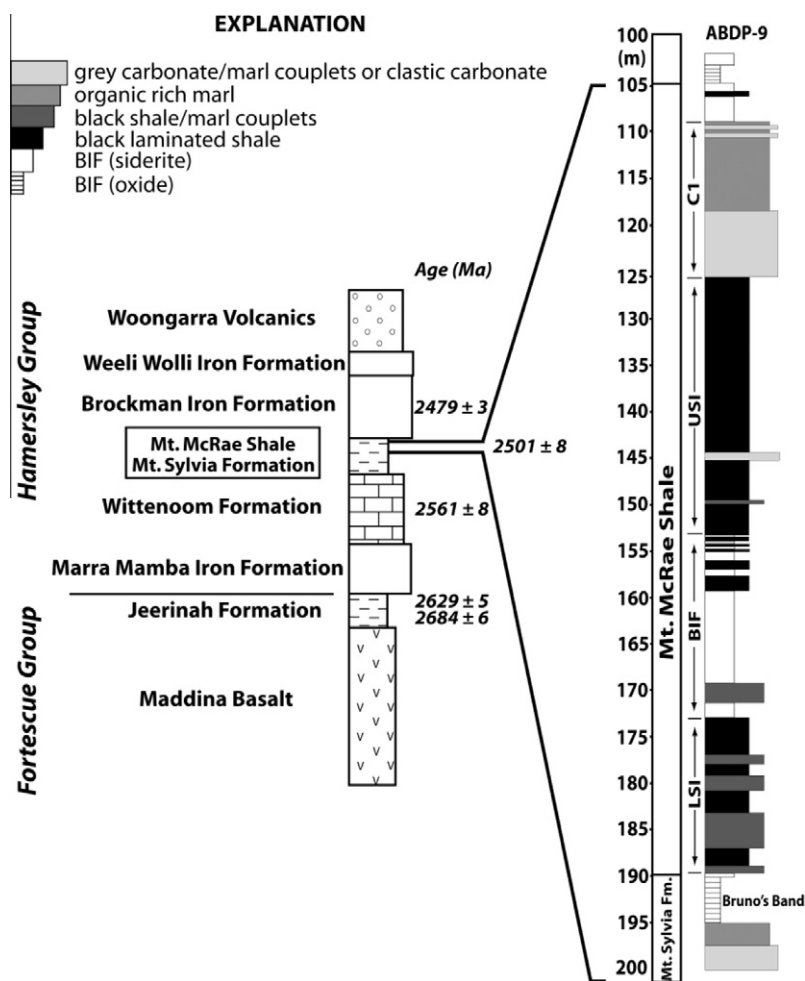


Fig. 1. Stratigraphic context for the ABDP-9 core. Radiometric age constraints from Ono et al. (2003) and Anbar et al. (2007). General stratigraphy adapted from Ono et al. (2003) and Kaufman et al. (2007). Figure modified from Reinhard et al. (2009).

Morris, 1993; Webb et al., 2003; Klein, 2005; Pecoits et al., 2009).

The Mt. McRae Shale is a mixture of chemically precipitated Fe-rich authigenic minerals (the chert–silicate–carbonate facies) with 30–60% terrigenous clastics (Alibert and McCulloch, 1993; Morris, 1993), but pyroclastics are thought to be absent (Webb et al., 2003). The shales in the Mt. McRae differ from those within the Dales Gorge Member principally by containing more organic C and pyrite, which are mainly accompanied by quartz, siderite, dolomite, ankerite/ferroan dolomite, chlorite, mica, K-feldspar, albite and minnesotaite (Kakegawa et al., 1999; Krapez et al., 2003; Pickard et al., 2004). Coarse-grained siderite and ferroan dolomite were formed during early diagenesis (Krapez et al., 2003). Thus, authigenic Fe in the Mt. McRae Shale is present as sulfide, carbonate and silicate minerals. Petrographic studies (Maynard, 1983; Kakegawa et al., 1999) have shown that pyrite can be found enveloped by carbonates (calcite, dolomite/ankerite and siderite). Laminae in the enclosing sediment also compact around pyrite grains, indicating formation in the bottom waters or in unconsolidated sediments close to the sediment surface. Pyrite formation must have preceded carbonate formation

but both phases formed close to the sediment surface and are syngenetic or early diagenetic (here defined to be where porewaters are still in contact with overlying seawater).

Siderite is widely accepted to precipitate directly by reactions between dissolved Fe and dissolved carbonate (Ewers and Morris, 1981; Klein and Beukes, 1989; Morris, 1993; Webb et al., 2003; Pecoits et al., 2009). Ferroan dolomite or ankerite almost invariably shows evidence for growth during diagenesis, but it is difficult to ascertain the timing of growth because both minerals have often been recrystallized (Krapez et al., 2003). These observations suggest that pyrite, calcite and siderite (and possibly also ferroan dolomite and ankerite) in the Mt. McRae Shale were precipitated from bottom waters or near-surface porewaters (Reinhard et al., 2009), as is generally believed to be the case for these minerals in the Dales Gorge Member (Klein and Bricker, 1977; McConchie, 1987; Krapez et al., 2003; Fischer and Knoll, 2009).

The precise origin and timing of iron silicate formation is less certain. Greenalite is generally accepted to be syngenetic or early diagenetic (Webb et al., 2003; Klein, 2005), forming from reactions between dissolved Fe^{2+} or $\text{Fe}(\text{OH})_3$ and dissolved or amorphous silica (Maynard, 1983; La-

Berge et al., 1987; Pecoits et al., 2009). Stilpnomelane may form by early diagenetic reactions between $\text{Fe}(\text{OH})_3$ and amorphous or dissolved silica (Klein and Bricker, 1977; Maynard, 1983; McConchie, 1987; LaBerge et al., 1987) but has also been suggested to be a late diagenetic or metamorphic alteration product of greenalite (Gole, 1980; Krapez et al., 2003). Minnesotaitite is believed to form by late diagenetic or metamorphic alteration of greenalite (Klein and Bricker, 1977; Gole, 1980; LaBerge et al., 1987; Webb et al., 2003; Klein, 2005; Pecoits et al., 2009). Chamosite is more aluminous and less stable than greenalite and may represent alteration of a clastic silicate precursor but the timing of alteration is unclear (LaBerge, 1966; Gole, 1981; Maynard, 1983). Overall, the formation and alteration of different iron silicates results from poorly quantified variations in seawater or porewater chemistry, and the composition and relative proportions of clastic and syngenetic precursor phases as well as in the degree of burial diagenesis and/or metamorphism.

3. ANALYTICAL METHODOLOGY

We used quantitative phase analysis (QPA) of random powder X-ray diffraction (XRD) patterns to determine the concentrations of mineral phases in the Mt. McRae Shale (Srodon et al., 2001; Omotoso et al., 2006). Fourteen samples were prepared for QPA by mixing with 10% ZnO and milling for 5 min with 6 ml hexane. After drying at 60 °C, the samples were sieved (0.4 mm) and side-loaded into an aluminum holder for disorientation. XRD patterns were obtained with a Siemens D5000 Diffractometer using Cu radiation over the range 5–65° 2 θ . Mineral abundances were estimated (Table 1) using single line quantification with full pattern fitting and pure minerals as standards for reference intensity ratios (Srodon et al., 2001). The accuracy of mineral quantification has been tested using artificial mixtures of known composition and proven to be accurate and precise (Omotoso et al., 2006). Mean relative errors are 5–10% for major minerals (>10 wt%) and ~30% for minor components (<5 wt%), and the detection

limit is <1%. Clay mineralogy is reported using the nomenclature of Brigattii et al. (2006).

The use of the iron proxies $\text{Fe}_{\text{HR}}/\text{Fe}_{\text{T}}$ and DOP in Archean and Proterozoic rocks has proved valuable in distinguishing anoxic, non-sulfidic water columns from sulfidic (euxinic) conditions (Shen et al., 2003; Poulton et al., 2004; Reinhard et al., 2009). However, these proxies require accurate determination of the iron present as sulfides, carbonates and oxides. Iron present as pyrite (Fe_{py}) was measured by a chromous chloride extraction (Canfield et al., 1986). Reinhard et al. (2009) performed extractions of carbonates and oxides using the sequential extraction technique of Poulton and Canfield (2005), which measures the iron present as carbonates by extraction with Na acetate at pH 4.5 for 48 h at 50 °C (Fe_{carb}), as oxides by extraction with dithionite at pH 4.8 for 2 h at room temperature (Fe_{ox}) and as magnetite by extraction with oxalate at pH 3.2 for 6 h at room temperature (Fe_{mag}). Hence, Fe_{HR} is defined as $\text{Fe}_{\text{carb}} + \text{Fe}_{\text{ox}} + \text{Fe}_{\text{mag}} + \text{Fe}_{\text{py}}$. However, the acetate extraction does not dissolve sideritic Fe quantitatively in some samples from the ABDP-9 core, and this siderite is partially extracted during the subsequent oxalate step (Reinhard et al., 2009). In this case a better approach to measuring sideritic Fe was suggested by the data of Raiswell et al. (1994) who found that, within analytical error, cold 10% HCl at room temperature for 24 h dissolved siderite and ankerite quantitatively. Ferrihydrite and lepidocrocite were also dissolved quantitatively, but goethite and hematite were essentially insoluble. Ferrihydrite and lepidocrocite are altered rapidly to goethite/hematite and are not found in ancient sediments (Cornell and Schwertmann, 2003). Hence the Fe extracted from ancient rocks by 10% HCl does not comprise well-ordered, crystalline Fe oxide minerals. Raiswell et al. (1994) also found that complete dissolution of siderite by cold 10% HCl was accompanied by the dissolution of 1–2% of iron from nontronite, chlorite and biotite and so the iron extracted (Fe_{HCl}) can be an over-estimation of Fe_{carb} in the presence of these iron silicates. Nevertheless we have found that a 24 h extraction with cold 10% HCl, once corrected for

Table 1
Quantitative XRD results.

Depth	Unit	Quartz	K-feldspar	Calcite	Siderite	Dolomite	Ankerite	Pyrite	Mica	Fe-rich chlorite + serpentine
109.00	C1	14.6	29.3	0.0	0.0	0.7	6.3	2.1	7.3	38.7
113.46	C1	17.2	26.3	0.0	0.0	5.1	3.0	1.0	36.4	10.6
121.2	C1	16.6	10.4	5.2	0.0	3.1	46.6	0.0	14.5	3.1
137.68	USI (pyl)	27.8	13.3	1.0	0.0	0.0	0.7	16.7	34.4	5.6
143.45	USI (pyl)	42.8	3.8	0.5	0.0	0.0	1.3	12.6	30.2	8.8
144.36	USI	40.3	10.9	6.5	0.1	0.0	1.1	4.4	15.3	20.7
149.3	USI	21.0	27.6	0.3	0.0	0.1	1.1	5.5	34.3	9.9
162.8	BIF	5.4	18.5	0.0	39.1	0.1	1.1	2.2	14.1	19.5
168.9	BIF	25.9	7.1	0.0	34.1	0.0	10.6	3.5	2.4	16.5
169.94	BIF	27.3	5.1	0.0	39.4	0.0	11.1	6.1	1.0	10.1
173.5	LSI	24.9	24.9	0.0	9.7	0.2	0.9	7.6	5.7	25.9
173.73	LSI	25.8	16.5	0.0	26.8	0.0	2.1	3.1	4.1	21.6
183.65	LSI	36.3	22.0	0.0	8.8	0.0	5.5	3.3	7.7	16.5
185.43	LSI	38.9	11.9	0.0	11.9	0.1	11.9	2.2	2.4	20.5

Presence of pyrite laminae indicated by pyl.

dithionite-soluble Fe ($Fe_{c-HCl} - Fe_{ox}$), produces the closest match between the carbonate equivalents (derived either from the sum of the metals extracted as Fe_{c-HCl} or $Fe_{c-HCl} - Fe_{ox}$) and independently measured values for inorganic carbon (C_{inorg}) (see below). An absolutely accurate measurement of Fe_{carb} in the presence of iron silicates may be impossible but our pragmatic approach is further evaluated below using a selection of iron silicates representative of those found in the Mt. McRae Shale. Our aim is to refine existing methodologies to optimize measurement of Fe_{carb} and hence allow the Fe present as reactive silicates to be estimated.

We utilize the Fe_{ox} and Fe_{py} data from Reinhard et al. (2009) here along with new Fe_{c-HCl} data to define Fe_{carb} as ($Fe_{c-HCl} - Fe_{ox}$) and Fe_{HR} as ($Fe_{c-HCl} + Fe_{py}$). We also present new data to extend the partition of Fe into silicate phases by using the boiling HCl extraction of Raiswell et al. (1994). This extraction was performed on fresh samples and the iron removed (Fe_{b-HCl}) is present in reactive silicates as well as carbonates (but not oxides which are absent in the Mt. McRae Shale, see later). Hence, Fe in reactive silicates (Fe_{sil}) is estimated as ($Fe_{b-HCl} - Fe_{carb}$). Iron in these extractions was measured on an Agilent 7500ce ICP-MS after 100-fold dilution in trace metal grade 0.36 M HNO_3 with a precision of 7% for replicate extractions.

The Fe speciation data were formulated into the proxies Fe_{HR}/Fe_T and DOP (weight ratios used here and throughout) that can distinguish between anoxic but non-sulfidic water columns and anoxic water columns containing free H_2S (euxinic) as outlined by Reinhard et al. (2009). The ratio Fe_{HR}/Fe_T averages 0.26 ± 0.08 in modern oxic sediments from the continental margin and the deep sea (Raiswell and Canfield, 1998) and values above 0.38 indicate an anoxic water column enriched in dissolved Fe. Dissolved sulfide and dissolved Fe cannot coexist in solution because iron sulfides are very insoluble, and Raiswell et al. (1988) define Degree of Pyritization (DOP) as $Fe_{py}/(Fe_{py} + Fe_{b-HCl})$, which recognizes that sulfidic water columns yield $DOP > 0.8$ (unless siliclastic accumulation rates are sufficiently high to dilute the pyrite formed by the shuttle enrichment of iron; Lyons and Severmann, 2006). Also high ratios of Fe_{py}/Fe_{HR} (Reinhard et al., 2009) point to euxinia when occurring with high Fe_{HR}/Fe_T .

Total carbon ($C_{tot} = C_{inorg} + C_{org}$) was measured by combustion at 1400 °C using an Eltra CS-500 Carbon Sulfur Determinator. Values for C_{inorg} were obtained as ($C_{tot} - C_{org}$). Data for C_{org} from Kaufman et al. (2007) were obtained by combustion following the complete dissolution of carbonates in concentrated HCl overnight at 65 °C.

4. RESULTS

4.1. Mineralogy

A selection of 14 samples spanning C1, USI, BIF and LSI was chosen for detailed mineralogical study by XRD. The mineral composition of these samples was highly variable (Table 1), but the samples separate into two major groups: C1 and USI contain little or no siderite but are rich

in mica, whereas BIF and LSI are siderite-rich and generally deficient in mica. Mica occurs as an Fe-poor, 2:1 layer dioctahedral phyllosilicate. Siderite in the USI and the BIF ranges between 9% and 39%.

A 2:1 + 1 phyllosilicate was identified as an Fe-rich chlorite. In several samples, mostly those from depths around 109 m, a trioctahedral 1:1 Fe-rich serpentine was also identified. However this mineral is structurally similar to Fe-rich chlorite, and it is difficult to distinguish the two minerals. The two minerals are therefore grouped together in Table 1. The total chlorite + tri 1:1 serpentine content tends to be highest in the LSI but varies irregularly from 3% to 39% through the section.

Ankerite/ferroan dolomite occur along with siderite. Dolomite is only present at low concentrations in C1 (Table 1), but the ankerite content varies irregularly. Ankerite concentrations are highest in C1 (up to 47%) but fall to only trace amounts in the USI (~1%), while concentrations are 1–12% in LSI and the BIF. Calcite was identified only in the USI and C1 at concentrations of <7%.

Feldspar is very abundant throughout the section and is present mainly as K-feldspar, and plagioclase is only present at minor concentrations close to the detection limit of <1%. Both feldspars are grouped together as K-feldspar in Table 1. Pyrite content varies from 0% to 17% with maximum values in the upper part of the USI. Hematite, magnetite, minnesotaite and stilpnomelane were below the detection limit (<1%) in all samples.

4.2. Iron speciation

In order to estimate the Fe present as carbonate, oxide, sulfide and silicate phases, we require the data for Fe_{ox} and Fe_{py} reported by Reinhard et al. (2009) plus our new determinations of Fe_{c-HCl} and Fe_{b-HCl} (see Electronic Annex). The estimates of Fe_{py} and Fe_{ox} rely only on single analytical measurements that are readily validated by reference to the XRD data (Table 1). The Fe_{py} data from Reinhard et al. (2009) are highly correlated ($r = 0.99$) with the XRD pyrite contents from Table 1, with a slope ($Fe_{py}/\text{pyrite content}$) of 0.44 that closely matches the stoichiometric value (0.46) for pyrite. Values of Fe_{ox} are uniformly low (0–0.5%), consistent with the XRD data (see above). The Fe_{carb} and Fe_{sil} estimates cannot be validated by reference to the XRD data because there are a variety of Fe-bearing carbonates and silicates, and their precise compositions are unknown.

The estimates of Fe_{carb} can be validated as follows. The data (Electronic Annex) show that Fe_{c-HCl} ranges from 0% to 16.3%, with the highest values generally occurring in the BIF where XRD data show that siderite is abundant (Table 1). We have tested the efficiency of the cold 10% HCl extraction procedure for carbonate contents on the full suite of Mt. McRae samples, and on the limited selection of samples for which there are XRD data. Firstly, Fig. 2 compares the estimates of the C_{inorg} (obtained as the difference between measurements of C_{tot} from combustion of the whole rock and the C_{org} from Kaufman et al., 2007) with the C_{inorg} determined by summing the carbonate equivalents (C_{inorg}^*) of ($Fe_{c-HCl} - Fe_{ox}$) plus cold 10% HCl-soluble Ca and Mg. The full suite of Mt. McRae data shows a good

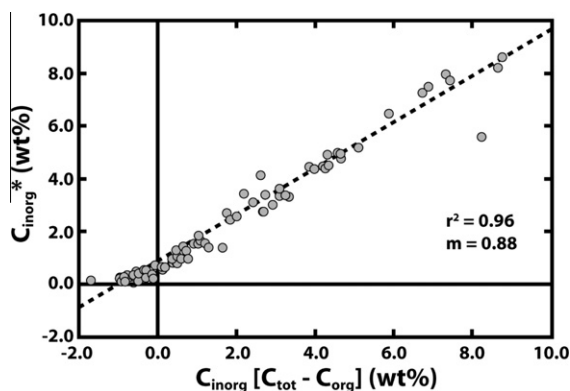


Fig. 2. Comparison of inorganic carbon concentrations obtained by summation of $(\text{Fe}_{\text{c-HCl}} - \text{Fe}_{\text{ox}})$ and cold HCl-soluble Ca and Mg ($\text{C}_{\text{inorg}}^*$) and by measurement of $(\text{C}_{\text{tot}} - \text{C}_{\text{org}})$.

linear correlation between $\%C_{\text{inorg}}$ derived by measurement of $(\%C_{\text{tot}} - \%C_{\text{org}})$ and $\%C_{\text{inorg}}^*$ calculated from the sum of $(\text{Fe}_{\text{c-HCl}} - \text{Fe}_{\text{ox}})$ plus cold HCl-soluble Ca and Mg (Fig. 2). Secondly, the limited set of samples with XRD data demonstrates that these two estimates (Table 2) are also in good agreement with the $\%C_{\text{inorg}}$ estimated by XRD, even in the sideritic samples of BIF and LSI. Small negative values occur for the $\%C_{\text{inorg}}$ derived by measurement in the USI because C_{org} content is high and $(\text{C}_{\text{tot}} - \text{C}_{\text{org}})$ is thus the difference between two large numbers. These negative values may indicate a small systematic under-estimation of C_{tot} or over-estimation of C_{org} . Overall the 10% HCl extraction is effective at dissolving the Ca, Mg and Fe-bearing carbonates in the Mt. McRae Shale and the small contributions from reactive silicates can be minimized by deriving Fe_{carb} from $(\text{Fe}_{\text{c-HCl}} - \text{Fe}_{\text{ox}})$. Below we examine how this methodology affects estimates of silicate Fe.

We proposed earlier to measure Fe present in reactive silicates as $\text{Fe}_{\text{b-HCl}} - \text{Fe}_{\text{carb}}$. As a step toward validating this approach, we determined $\text{Fe}_{\text{c-HCl}}$, $\text{Fe}_{\text{b-HCl}}$ and Fe_{ox} on museum-grade Fe-rich chlorite, Fe-rich serpentine, Fe-rich mica and Fe-rich talc selected to represent iron silicates

typically found in BIF and associated shales (see above). We picked out material showing surface oxidation prior to analysis. We measured extracted Fe with a precision of 7.5% by colorimetry using a hydroxylamine reducing agent to convert Fe^{3+} to Fe^{2+} in conjunction with the ferrozine colorimetric reagent (Stookey, 1970). Total Fe (Fe_{T}) and Al were measured by XRF with precisions of 5% and 2%, respectively. Analytical data are reported in Table 3.

Unfortunately, there was insufficient Fe-rich talc to obtain XRF data and the Fe_{T} and Al data were inferred from the compositions determined by Gole (1980) and Webb et al. (2003) in BIF. The boiling HCl treatment removes essentially all the Fe (within analytical error) from Fe-rich serpentine, Fe-rich mica and Fe-rich talc but only ~25% of the Fe in Fe-rich chlorite. The dithionite extraction removes <1% Fe from Fe-rich chlorite and Fe-rich mica and 2–3% Fe from Fe-rich serpentine and Fe-rich talc. Cold 10% HCl dissolved more Fe (1–2%) from Fe-rich mica and Fe-rich chlorite and substantially more from Fe-rich serpentine. These data indicate that there is a significant overlap in the reactivity of siderite and silicate Fe and hence their accurate distinction is difficult and critically dependent on mineralogy. Our measurements of Fe_{carb} as $(\text{Fe}_{\text{c-HCl}} - \text{Fe}_{\text{ox}})$ in ABDP-9 includes all sideritic Fe plus some silicate Fe (that soluble in cold HCl but not dithionite). It follows that measurement of reactive silicate Fe as $(\text{Fe}_{\text{b-HCl}} - \text{Fe}_{\text{carb}})$ may be underestimated due to the presence of silicate Fe in Fe_{carb} but this error will only be small unless large amounts of greenalite are present. In any event, reproducible measurements allow us to distinguish changes throughout the sequence (see discussion).

We can define an authigenic Fe component in two ways. The first is by estimating a terrigenous Fe component using the $\text{Fe}_{\text{T}}/\text{Al}$ ratio. Raiswell et al. (2008) determined a mean $\text{Fe}_{\text{T}}/\text{Al}$ ratio of 0.53 ± 0.11 for Paleozoic shales that were deposited in an oxygenated depositional environment (thus excluding euxinic and ferruginous sediments where iron enrichments occur; Canfield et al., 1996; Raiswell and Anderson, 2005; Lyons and Severmann, 2006). This mean $\text{Fe}_{\text{T}}/\text{Al}$ ratio overlaps with the range of values found in

Table 2
Comparison of C_{inorg} determinations by different methods.

Depth	Unit	$\%C_{\text{inorg}} =$ $\%C_{\text{tot}} - \%C_{\text{org}}$	$\%C_{\text{inorg}}^*$ equivalents of metals extracted by cold 10% HCl (Fe_{carb} , Ca and Mg)	Min% XRD	Max% XRD
109	C1	0.65	1.43	0.6	1.2
113.46	C1	0.78	0.95	0.6	1.4
121.2	C1	6.74	7.25	6	7.7
137.68	USI	-0.95	0.25	0.1	0.4
143.45	USI	-0.6	0.21	0.1	0.4
144.36	USI	0.37	0.81	0.7	0.9
149.3	USI	-0.86	0.27	0.1	0.4
162.8	BIF	4.21	4.46	3.1	4.4
168.9	BIF	4.66	4.75	3.6	5.1
169.94	BIF	4.58	4.98	4.3	6.0
173.5	LSI	1.3	1.39	0.9	1.3
173.73	LSI	3.1	3.62	2.3	3.5
183.65	LSI	1.21	1.54	1.0	1.7
185.43	LSI	2.68	2.74	2.1	2.9

The XRD range arises from the variable C_{inorg} contents of carbonate minerals and represents an over-estimate.

Table 3
Dithionite and hydrochloride acid-extractable iron contents of iron silicate minerals.

Mineral	%Fe _{ox}	%Fe _{c-HCl}	%Fe _{b-HCl}	%Fe _T	%Al
Fe-rich chlorite (chamosite)	0.51	1.90	4.7	17.6	9.84
Fe-rich serpentine (greenalite)	2.35	14.3	24.5	24.0	6.86
Fe-rich mica (stilpnomelane)	0.70	1.11	24.7	22.5	2.46
Fe-rich talc (minnesotaite)	2.46	NA	26.6	23.9–28.0	0.14–0.66

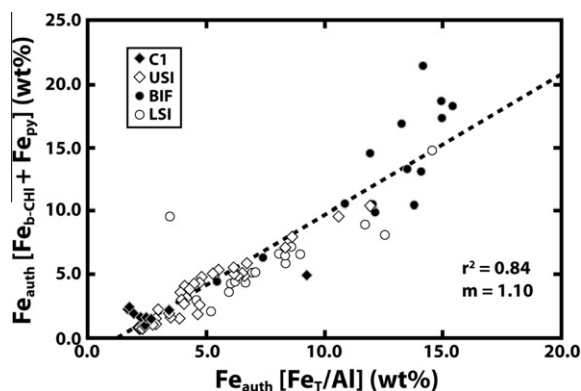


Fig. 3. Relationship between authigenic Fe (Fe_{auth}) determined as $Fe_{b-HCl} + Fe_{py}$ and as $Fe_T - 0.53 * Fe_T/Al$.

average shale (0.50–0.56; Clarke, 1924; Ronov and Migdissov, 1971; Taylor and McLennan, 1985) and the value of 0.48 from Proterozoic igneous rock composites used by Kump and Holland (1992) to assess Fe enrichments. Hence we can define an authigenic Fe component (Fe_{auth}) as:

$$Fe_{auth} = Fe_T - \frac{0.53 * Fe_T}{Al},$$

which quantifies the addition of Fe to the Mt. McRae Shale over and above that typically present in clastic and/or igneous source rocks. This enrichment in Fe must occur as primary or diagenetic minerals and hence Fe_{auth} can also be estimated by summing the Fe present as pyrite, oxides, carbonates and reactive silicates (or $Fe_{b-HCl} + Fe_{py}$). These two measurements of authigenic Fe fall on a reasonably well-defined straight line ($r^2 = 0.85$; Fig. 3) described by:

$$(Fe_{b-HCl} + Fe_{py}) = 1.1 * [Fe_T - (0.53 * Fe_T/Al)] - 1.6.$$

Fig. 3 also indicates that Fe_{b-HCl} provides a good measure of authigenic carbonate and silicate Fe over the diagenetic timescales involved.

5. INTERPRETATION

5.1. Constraints from carbonate, sulfide and silicate equilibria

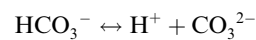
The iron speciation data quantify the occurrence of authigenic carbonate, sulfide and silicate minerals in the Mt. McRae Shale that are controlled ultimately by Archean seawater chemistry. Here we explore the qualitative constraints on the iron speciation data that are provided by considering the carbonate, sulfide and silicate equilibria in relation to the relative abundances of the main cationic

and anionic species. The chemistry of Precambrian seawater has been discussed by Walker (1983) and Grotzinger and Kasting (1993), who examined the relationship between atmospheric pCO_2 and seawater pH following the approach of Holland (1984). These studies and others (Rye et al., 1995; Ohmoto et al., 2004) suggest a range of pCO_2 from 0.03 to 0.3 atm. An ocean saturated with respect to calcite and siderite and in equilibrium with $pCO_2 = 0.03$ atm requires a seawater pH of 7.1–7.4, and $pCO_2 = 0.3$ atm requires a seawater pH of 6.6–6.9. Walker (1983) and Grotzinger and Kasting (1993) estimated alkalinity as 1–10 mM, dissolved $[Fe^{2+}] \sim 1$ –3 ppm (20–50 μM) and dissolved $[Ca^{2+}] \sim 3$ –9 ppm (8–20 μM). Somewhat higher concentrations of dissolved Fe^{2+} (40–120 μM) have been suggested by Canfield (2005). Magnesium occurs in dolomite, ankerite and siderite and precipitation is controlled by relative saturation with respect to these minerals. The above estimates indicate $\Sigma[Fe^{2+} + Ca^{2+}] \ll [HCO_3^-]$ in Precambrian seawater and hence precipitation of syngenetic and early diagenetic carbonate minerals in contact with the relatively large alkalinity reservoir in seawater will be limited by cation supply.

Consider the closed system precipitation of Ca^{2+} and Fe^{2+} as carbonates:



Precipitation of 140 $\mu moles$ of $Fe^{2+} + Ca^{2+}$ (the sum of the maximum concentrations estimated in Precambrian seawater) is accompanied by the removal of 140 $\mu moles$ of bicarbonate irrespective of mineralogy. An examination of the carbonate equilibria (using apparent dissociation constants for seawater from Millero, 2001) shows that this removal of HCO_3^- produces a negligible change in pH and $[CO_3^{2-}]$ for an equilibrium system at 25 °C even with a relatively low concentration of $[HCO_3^-] = 1$ mM. Consider the $HCO_3^- - CO_3^{2-}$ equilibria before precipitation:



$$10^{-8.92} = \frac{\{H^+\}\{CO_3^{2-}\}}{[HCO_3^-]}$$

$$[CO_3^{2-}]\{H^+\} = 10^{-11.92}.$$

After the removal of 140 $\mu moles$ of $[HCO_3^-]$ by precipitation, the product $[CO_3^{2-}] * \{H^+\}$ only declines to $10^{-11.99}$. Precipitation of twice the concentrations of cations (and HCO_3^-) only changes the product $[CO_3^{2-}] * \{H^+\}$ to $10^{-12.06}$. Hence the carbonate system is well buffered against changes induced by precipitation in a closed system even when assuming relatively large estimates of cation concentrations. Syngenetic and early diagenetic carbonate

precipitation in an open system will therefore be mainly controlled by changes in cation concentrations, which have a much larger effect on the carbonate saturation state than do changes in $[\text{HCO}_3^-]$ and $\{\text{H}^+\}$.

The Fe silicate equilibria can be examined in the same way as the carbonate equilibria in order to show that the saturation state of Fe silicates is also controlled by cation concentrations. The direct precipitation of Fe-rich serpentine:



releases H^+ (as does carbonate precipitation), which is also well buffered by the carbonate equilibria (see above). Tardy and Garrels (1974) give a $\Delta G = -3012$ kJ for an idealized Fe-rich serpentine with the composition $\text{Fe}_3\text{Si}_2\text{O}_5(\text{OH})_4$. Using additional thermodynamic data from Woods and Garrels (1987), an equilibrium constant can be derived for Fe-rich serpentine precipitation as:

$$K = 10^{-16.7} = \frac{\{\text{H}^+\}^6}{\{\text{Fe}^{2+}\}^3 \{\text{H}_4\text{SiO}_4\}^2}.$$

Assuming seawater pH 7 and dissolved silica in equilibrium with amorphous silica (at ~ 2 mM), the above equation indicates that the saturation activity of $\{\text{Fe}^{2+}\} = 0.25$ μM (or 1 μM with 0.2 mM dissolved silica) for equilibrium with Fe-rich serpentine. Waite (2001) presented data that enable activity-concentration effects to be estimated. The speciation of Fe(II) in modern seawater at pH 8 and 25 °C is predominantly Fe^{2+} (43%) with smaller contributions from the ion pairs FeCO_3^0 (34%), FeCl^+ (15%) and FeSO_4^0 (5%). The FeSO_4^0 ion pair can be ignored in sulfate-poor Precambrian seawater and, as the pH falls to 7.5, the carbonate ion pair accounts for <1% of the Fe(II) species and at pH 6.6 (the minimum for Precambrian seawater, see earlier) $\text{FeCO}_3^0 < 0.1\%$. The higher alkalinities in Precambrian seawater do not significantly change the relative species abundances and $\text{Fe}^{2+} > \text{FeCO}_3^0$ and the speciation is dominated by Fe^{2+} , which is approximately 3 \times more abundant than FeCl^+ . Hence in Precambrian seawater the total concentration of Fe^{2+} is approximately $\{\text{Fe}^{2+}\}/\gamma_{\text{Fe}}$, where γ_{Fe} is the activity coefficient of Fe^{2+} in seawater (~ 0.26 ; Millero, 2001). Dissolved Fe concentrations are thus only about 4 \times higher than $\{\text{Fe}^{2+}\}$ and activity-concentration effects are not large in relation to the estimated range of dissolved Fe^{2+} (~ 10 – 100 μM). Thus the iron silicate system, like the iron carbonate system, would be at saturation with relatively low concentrations of dissolved Fe (~ 10 – 100 μM) compared to dissolved silica concentrations and precipitation can be considered to respond principally to increases in dissolved iron concentrations in bottom waters. The silicate equilibria are poorly constrained but also suggest that contemporaneous supersaturation may be achieved for iron silicates as well as siderite.

The sulfide equilibria behave quite differently. Syngenetic or early diagenetic pyrite is present throughout the Mt. McRae Shale (see Table 1) and so it is reasonable to assume that bottom waters were at or near-saturation with amorphous FeS which is typically precipitated before, and is less soluble than, pyrite (Rickard and Luther, 2007). Previous considerations of sulfide equilibria have argued

that the solubility product of amorphous FeS is so low that saturation with respect to FeS in waters with 10–100 μM dissolved Fe (see above) requires only very low concentrations of dissolved sulfide (at least an order of magnitude lower; Canfield and Raiswell, 1991). This observation still holds in acid to neutral waters although the complex FeS^0 has been shown to be important at higher pH (Rickard and Luther, 2007) where this species may carry equivalent concentrations of dissolved Fe and sulfide (if both are present at micromolar levels). The lower pH and higher dissolved Fe concentrations of the Precambrian ocean (see above), however, indicate that saturation with amorphous FeS kept dissolved sulfide at low levels and hence $\Sigma[\text{Fe}^{2+}] \gg \Sigma[\text{S}^{2-}]$. The sulfide system, in contrast to the silicate and carbonate systems, is significantly more responsive to changes in anion concentrations (i.e. dissolved sulfide). As such there are two main factors that defined the response of the anoxic Mt. McRae basin to changes in the seawater chemistry at near-saturation with siderite, iron silicates and FeS: (1) increases in SO_4^{2-} followed by reduction to sulfide and precipitation as FeS and (2) increases in dissolved Fe followed by precipitation of iron silicates and iron carbonates but only limited formation of iron sulfide.

5.2. Variations in water-column chemistry

Reinhard et al. (2009) suggested that the Mt. McRae Shale was deposited from a water column that always contained dissolved Fe below a shallow (probably oxic; Kendall et al., 2010) surface layer, except during deposition of the USI which accumulated a zone of mid-water column euxinia. These basin-scale features of water-column chemistry are shown in Fig. 4a, which shows that the Mt. McRae section can be divided into two parts based on DOP.

The lower part of the sequence from 190 to 153 m spanning the LSI and the BIF has DOP values < 0.8 and values of $\text{Fe}_{\text{HR}}/\text{Fe}_{\text{T}} > 0.38$ (Raiswell and Canfield, 1998) which indicate the presence of an anoxic, iron-rich water column (Reinhard et al., 2009). By contrast, DOP values > 0.8 in the USI (depths 153–133 m) indicate euxinic bottom waters (Raiswell et al., 1988). These data provide an important distinction between a lower section with an iron-rich water column and an upper part with a sulfidic water column (Reinhard et al., 2009). This distinction exerts an important control on mineralogy, with the abundance of dissolved iron remaining after pyrite formation controlling the subsequent formation of siderite and iron silicates.

We now examine the evidence for iron enrichment by comparing the $\text{Fe}_{\text{T}}/\text{Al}$ ratio (Lyons and Severmann, 2006) through the sequence (Fig. 4b) to the mean value in Paleozoic shales (0.53 ± 0.11 ; Raiswell et al., 2008). These data define a prominent peak ($\text{Fe}_{\text{T}}/\text{Al} > 2$) from ~ 175 to 163 m in the BIF and a region from ~ 146 to 135 m in the USI where there is evidence for erratic iron enrichments ($\text{Fe}_{\text{T}}/\text{Al}$ mostly > 1). The LSI has a mean $\text{Fe}_{\text{T}}/\text{Al}$ of 1.9 ± 0.9 , and the overlying BIF has an average $\text{Fe}_{\text{T}}/\text{Al}$ of 4.7 ± 2.9 . $\text{Fe}_{\text{T}}/\text{Al}$ ratios fall to 0.66 ± 0.13 above the BIF through the lowest part of the USI (153.18–147.3 m), before rising to 1.3 ± 0.7 through 146–135 m where the

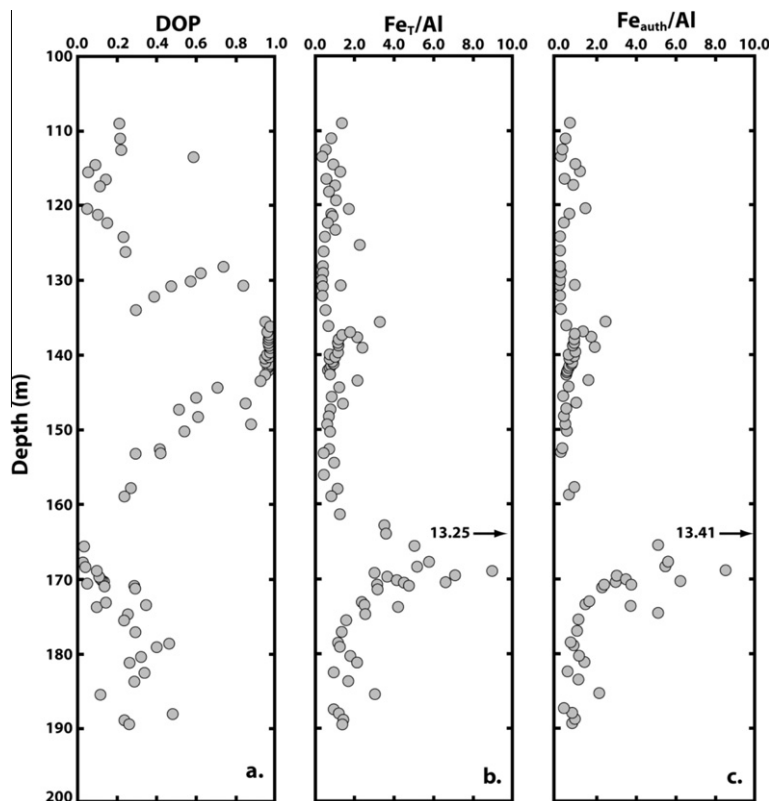


Fig. 4. Stratigraphic variations in (a) DOP, (b) Fe_T/Al and (c) Fe_{auth}/Al .

erratic peaks occur. Above this, in the uppermost region of the USI, the Fe_T/Al falls to 0.50 ± 0.30 and rises again to 1.0 ± 0.5 in the carbonate. The mean Fe_T/Al values of the upper and lower regions of the USI are not significantly different (at the $<1\%$ level) to mean Paleozoic shale. However, the BIF and region of high Fe_T/Al in the USI from 146 to 135 m are both significantly Fe-enriched compared to Paleozoic shale (a ‘Student’s t test showed that the probability p of no significant difference was $<1\%$) and also significantly enriched compared to their adjacent sediments (at the $p < 1\%$ level). The stratigraphic variations in Fe_{auth} (Fig. 4c) confirm that these two parts of the section with high Fe_T/Al are also enriched in authigenic Fe. In the USI authigenic Fe contents reach 10% and coincide with high DOP, whereas in the BIF DOP values are low but Fe_{auth} reaches 20%.

It is tempting to attribute both these regions of Fe enrichment to the addition of hydrothermal Fe, but enrichments in Fe_T/Al are also characteristic of sulfidic basinal sediments where iron has been remobilized from an oxic shelf and exported to the deep basin for precipitation as sulfide (Lyons and Severmann, 2006; Raiswell, 2006; Severmann et al., 2008). This export of reactive iron is termed an iron shuttle and occurs where dissolved Fe(II) in shelf porewaters is mixed into the water column and oxidized to iron (oxyhydr)oxides that are advected to the deep basin. A literature survey of modern and ancient euxinic sediments (Fig. 5) shows that maximum Fe_T/Al are commonly 1–2 and do not exceed 2.8 (provided $Al > 0.5\%$). Very high

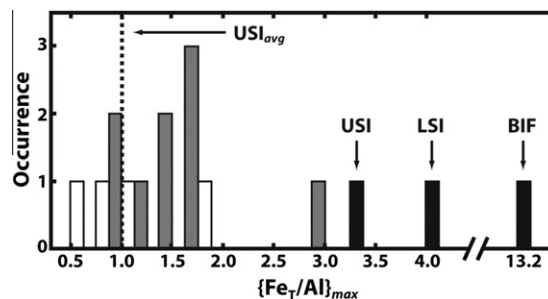


Fig. 5. Maximum Fe_T/Al values in modern (unshaded) and ancient (gray) euxinic sediments compared to the Mt. McRae Shale (black). Data for the Otaka Creek Formation from Werne et al. (2002), the Hushpuckney and Tackett Shales from Cruse and Lyons (2004), the Alum and Posidonia Shales and the Jet Rock from Gill (2009), the Stark Shale from Hatch and Leventhal (1992), the La Luna Formation from Mongenot et al. (1996), the Kimmeridge Clay from Tribouillard et al. (1993), the Black Sea, Effingham Inlet and Orca Basin from Lyons and Severmann (2006), Framvaren from Raiswell and Canfield (1998), and Mt. McRae USI, LSI, and BIF from Anbar et al. (2007). Average value in the USI shown by the dotted line. Note the scale break along the x-axis.

Fe_T/Al values are found in sediments where the aluminosilicate content is low but this is clearly not the case in the upper Mt. McRae Shale, which shows an average Fe_T/Al value of ~ 1 . Thus, enrichment by an Fe shuttle for the region 146–135 m in the USI is consistent with the DOP data

in Fig. 4a and the presence of sulfidic bottom waters as suggested by Reinhard et al. (2009). By contrast, the prominent Fe_T/Al in the BIF represents an exceedingly large Fe enrichment. It is highly significant that no Fe_T/Al values >2.8 have been observed to occur in modern or ancient euxinic sediments (see Fig. 5) and we therefore interpret the Fe_T/Al peak approaching 13 in the BIF as demonstrating the presence of bottom waters enriched in dissolved iron derived from hydrothermal activity.

5.3. Variations in sediment chemistry

5.3.1. C_{org} content

On a basinal scale the sediments comprising the Mt. McRae Shale represent a complex interplay between rates of precipitation of authigenic Fe-rich minerals sourced from dissolved Fe in the water column and rates of clastic sedimentation, which act to dilute the authigenic mineral content. Isolating the influence of these different processes is difficult because Al plays a dual role - as a diluent of authigenic phases and as a proxy for rates of siliclastic sedimentation. The Mt. McRae Shale started as fine-grained clastic debris that appears to have been deposited without any observable breaks in sedimentation. The major Al-bearing phases (feldspar, mica plus some iron silicates) are all either detrital, or derived from detrital precursors, and hence we can consider differences in Al content to reflect variations in rates of siliclastic sedimentation rates relative to the rate of addition of authigenic minerals.

In these circumstances the effects of dilution and sedimentation rate can be isolated by plotting elemental ratios to Al against Al content. For example an element E that is added to the sediment by processes that are coupled to the addition of Al-bearing clastics will have a constant E/Al ratio, even though Al may decrease through dilution by the addition of authigenic minerals. Conversely, the ratio E/Al will increase as the Al content decreases (or E increases) when element E is added by authigenic mineral formation and is decoupled from the clastic flux. In this case the decrease in Al is due to the dilution of the clastic content by authigenic minerals. Fig. 6 shows the variations in the ratio of C_{org}/Al in the Mt. McRae shale. The ratio of C_{org}/Al for LSI, BIF and C1 (mostly) remains uniform as the Al con-

tent decreases from 8% to 2%. Thus over this range rates of C_{org} deposition are coupled to rates of clastic deposition until $<2\%$ Al is being delivered to the sediment. However, the USI shows a rough trend of increasing C_{org}/Al with decreasing siliclastic delivery. Reinhard et al. (2009) suggested that the USI was deposited in the presence of a mid-water column sulfidic zone overlying dissolved Fe-rich bottom waters. Anoxic, dissolved Fe-rich bottom waters were also present during deposition of the LSI, BIF and C1 intervals but do not correspond to enrichments in C_{org}/Al . The similarity in bottom water conditions and resulting burial history for the LSI, BIF, USI and C1 suggests that preservation was similar throughout the section. It is therefore more likely that the C_{org} enrichments in the USI resulted from enhanced productivity, which produced the mid-column euxinia, rather than improved preservation (see below).

5.3.2. Total iron and highly reactive iron content

The Fe_T/Al data plotted against Al content (Fig. 7a) show two trends; a steep increase in Fe_T/Al seen in the BIF and in most of the USI and LSI samples, and a weaker increase in C1. Note that the convergence of the two trends occurs in a region where Al content is $\sim 8\%$ and Fe_T/Al is 0.4–0.55 (which approximates the mean Fe_T/Al in Paleozoic shales; see above). The steep trend to high Fe_T/Al values for the USI, BIF and LSI suggests that the increasing Fe_T/Al is due to the precipitation of increasing amounts of authigenic Fe minerals (caused by the addition of hydrothermal Fe, see above) to decreasing amounts of clastics with $Fe_T/Al \sim 0.5$. The weaker trend in C1 is similarly attributable to the addition of Fe_T (but in much smaller concentrations) to a clastic flux with the same Fe_T/Al content. The differences in the amounts of Fe_T added in C1 as compared to the USI, BIF and LSI may reflect differences in the rates of authigenic Fe mineral formation relative to the rates of clastic sedimentation. Fig. 7b confirms this possibility by showing that the Fe_{HR} content remains essentially uniform in C1 and the upper non-pyritic part of the USI. The rate of Fe_{HR} addition in these samples remains uniform at $\sim 1\text{--}2\%$ as the carbonate content increases and there is a decreasing contribution from a clastic component with a uniform Fe_T/Al . In contrast, the steep increase in Fe_{HR} in the BIF and LSI arises from an increasing addition of Fe_{HR} (mainly as carbonate) which dilutes the clastic flux. The same trends are seen in plotting Fe_{carb}/Al against Al (Fig. 7c). Clearly, the relative balance between authigenic Fe mineral formation and clastic sediment delivery is the main control on the abundance of Fe_{HR} , Fe_{carb} , silicate Fe (Fe_{sil}) and Fe_T .

5.3.3. Silicate Fe

Silicate Fe is low in the USI and C1 and, with the exception of one sample, also in the LSI and the Fe_{sil}/Al ratio is close to zero in these samples. However, significant concentrations of Fe_{sil} (3–4 wt%) are found in the BIF. The delivery of a fine aluminous ash from a distal volcanic source has been suggested to produce the chert–carbonate–silicate association in BIF (Ewers and Morris, 1981; Morris, 1993). Direct evidence of volcanic input is minimal

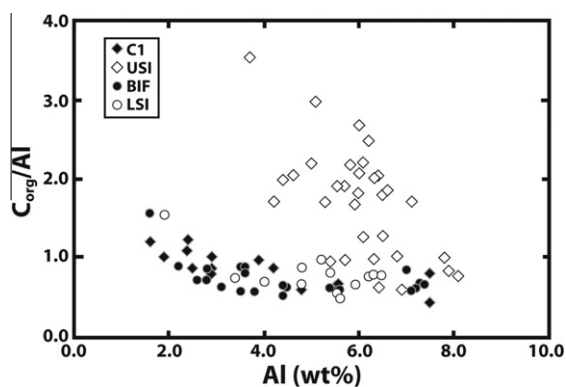


Fig. 6. Variations in C_{org}/Al with lithology in the Mt. McRae Shale.

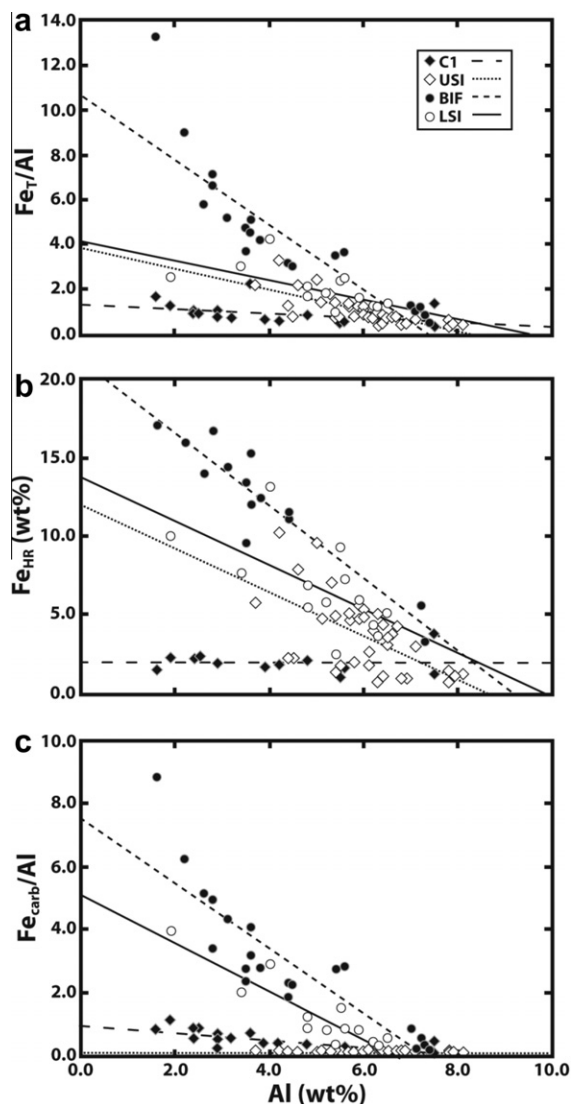


Fig. 7. Fe species variations as a function of Al content in the Mt. McRae Shale. Lines represent linear regressions for each unit. (a) Fe_T/Al ; r^2 values are 0.14 (C1), 0.76 (BIF), 0.39 (LSI), and 0.57 (USI). (b) Fe_{HR} content; r^2 values are 0.45 (C1), 0.75 (BIF), 0.81 (LSI), and 0.47 (USI). (c) Fe_{carb}/Al ; r^2 values are 0.57 (C1), 0.81 (LSI), 0.77 (BIF), and 0.004 (USI).

although rare volcanic shards have been identified in shaley beds (LaBerge, 1966). Webb et al. (2003) concluded that the black shales of the Mt. McRae Shale were undoubtedly deposited through non-volcanogenic processes. Our data (Fig. 8) show no evidence for any coupling between Fe_{sil} and Al that would be expected if Al-bearing dust were a significant source of reactants for the precipitation of Fe silicates. Instead, the pattern in Fig. 8 is similar to that in Fig. 7a–c and increasing values of Fe_{sil}/Al occur as the rate of addition of authigenic Fe increases relative to the rate of clastic Al delivery. There is also a weak correlation ($R = 0.42$) between Fe_{sil} and Fe_{carb} (Fig. 9) which confirms that authigenic iron silicates are present and indicates that increases in dissolved Fe caused the simultaneous precipitation of Fe_{carb} and Fe_{sil} (consistent with the equilibria con-

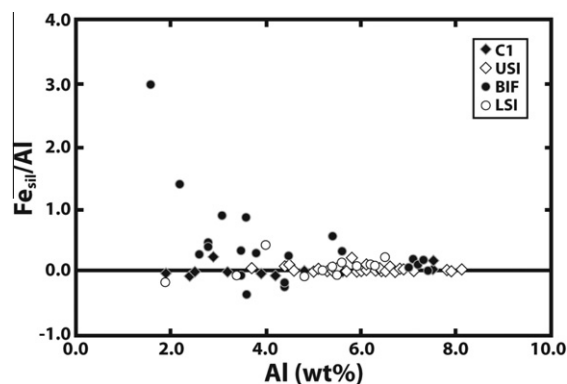


Fig. 8. Variations in Fe_{sil}/Al as a function of Al content in the Mt. McRae Shale.

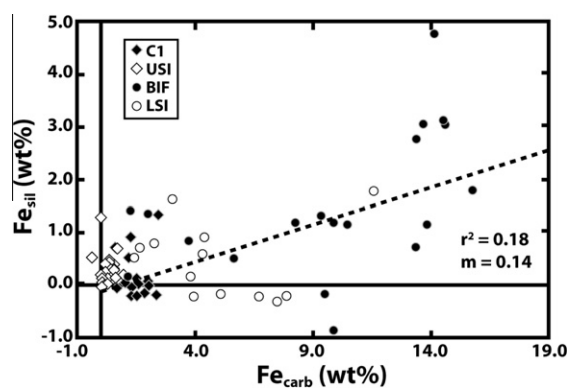


Fig. 9. Variations in Fe_{sil} as a function of Fe_{carb} content in the Mt. McRae Shale.

siderations). This data further indicate that 3–10 times more Fe was precipitated as siderite than silicate.

5.3.4. Pyrite iron

Variations of pyrite Fe display a different pattern to those of carbonate and silicate Fe. Plots of Fe_{py}/Al against Al do not display the simple linear trends seen in Fig. 7a–c for authigenic Fe, and the behavior of Fe_{py} is seen most clearly by separating the authigenic Fe into its component parts of Fe_{b-HCl} and Fe_{py} (Fig. 10). This plot shows a

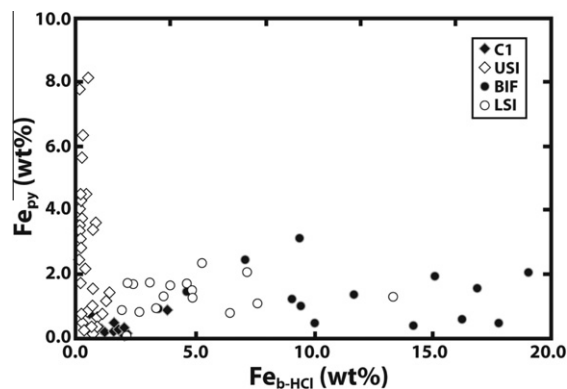


Fig. 10. Variations in Fe_{py} as a function of Fe_{b-HCl} content in the Mt. McRae Shale.

horizontal trend of Fe_{py} varying from 0% to 3% in the LSI, BIF, and C1, while Fe_{b-HCl} increases to nearly 20%. In contrast, the data from the USI plot vertically with variations in Fe_{py} from 0% to 10% being associated with negligible concentrations of Fe_{b-HCl} . Hence, the pyritic intervals in the Mt. McRae Shale contain low to negligible concentrations of iron carbonates and silicates because the insolubility of iron sulfide species prevented dissolved Fe^{2+} from coexisting with dissolved H_2S . In other words, dissolved Fe^{2+} concentrations were buffered to levels that were insufficient to stabilize other iron phases. In contrast, the non-pyritic sediments are characterized by a greater abundance of authigenic iron carbonates and silicates.

6. SYNTHESIS AND CONCLUSIONS

The use of the iron proxies Fe_{HR}/Fe_T and DOP have been proven in studies of Archean and Proterozoic rocks for distinguishing anoxic, non-sulfidic (ferruginous) water columns from sulfidic (euxinic) conditions (Shen et al., 2003; Poulton et al., 2004; Reinhard et al., 2009). Optimal use of these proxies requires accurate determination of the iron present as carbonate, oxide, sulfide and silicate. The sequential extraction scheme of Poulton and Canfield (2005) quantifies the iron present as carbonate minerals by extraction with Na acetate at pH 4.5 but we have found that Na acetate is not effective at dissolving siderite quantitatively from the Mt. McRae Shale, and the undissolved siderite carries over into subsequent extractions. This observation leads to the important conclusion that the methodology needs to be tested carefully on a case-by-case basis.

We have developed a methodology appropriate for the Mt. McRae Shale that includes the extraction of siderite and other Fe-rich carbonates by cold 10% HCl. This extraction of Fe_{c-HCl} is reasonably selective in that the only oxides dissolved are ferrihydrite and lepidocrocite (which are absent from the Mt. McRae Shale) but has little effect on iron silicates that are mineralogically similar to those found in the Mt. McRae Shale and are common in many BIFs. We have found that small amounts of Fe (1–2%) are removed from Fe-rich chlorite, Fe-rich mica and Fe-rich talc, but large amounts (~14%) are extracted from Fe-rich serpentine. We emphasize that these silicate extraction data are only approximations and the large compositional differences in these silicates are likely to cause differences in the amounts of Fe extracted. These differences can only be corrected on an individual basis. Nevertheless careful attention to mineralogy and extraction specificity will generally allow sideritic Fe to be measured reasonably accurately.

We have partially corrected our Fe_{c-HCl} data for the dissolution of silicate by using a dithionite extraction at pH 4.8 (Fe_{ox}); thus we determine Fe_{carb} as $(Fe_{c-HCl} - Fe_{ox})$. Dithionite removes less Fe from Fe-rich chlorite, Fe-rich mica, Fe-rich talc and Fe-rich serpentine than does cold 10% HCl but the correction optimizes the agreement between the carbonate equivalents plotted in Fig. 2. We recommend that the efficiency of carbonate extractions should be tested by reference to independent measures of C_{inorg} . An extraction using boiling HCl (Fe_{b-HCl}) enables reactive Fe present as authigenic silicates to be determined

as $Fe_{b-HCl} - Fe_{carb}$ where oxide Fe is absent, as in the Mt. McRae Shale. The iron speciation scheme refined for the Mt. McRae Shale measures the iron present as carbonate, sulfide and reactive silicates with an improved degree of selectivity that is confirmed by quantitative XRD analysis of the mineralogy.

The Mt. McRae Shale in core ADBP-9 records dramatic variations in lithology that occur in response to variations in basin chemistry tied to the relative additions of hydrothermal Fe, dissolved sulfate and continentally derived clastics. The lower part of the sequence through the lower shale interval (LSI) and BIF have elevated values of Fe_T/Al (>3) that are significantly above baseline levels of ~ 0.53 (as exhibited by Paleozoic oxic shales). Such exaggerated enrichments record pulses of hydrothermal Fe (Fig. 4a) that were removed mainly by reaction with dissolved carbonate to form siderite. There is a weak correlation between Fe_{carb} and Fe_{sil} , which is most apparent in the BIF (Fig. 9) and which implies that the abundances of both siderite and Fe-rich chlorite were controlled directly or indirectly by the availability of hydrothermal Fe. This conclusion is consistent with equilibrium considerations. Fe-rich chlorite may have formed by diagenetic alteration of Fe-rich serpentine or by reaction of dissolved iron with precursor clastic weathering products (see Velde, 2003). The relationship between Fe_{carb}/Al and Al (and to a lesser extent Fe_{sil}/Al and Al ; see Figs. 8 and 9) through the LSI and BIF show steep inverse trends that demonstrate that the enrichment of authigenic Fe in the sediments increases relative to rates of siliclastic sediment delivery. We conclude that the formation of both siderite and Fe-rich chlorite was controlled by rates of hydrothermal Fe addition relative to rates of clastic sediment delivery (see also Reinhard et al., 2009).

In contrast, the concentration of pyrite remains fairly uniform at ~ 1 –3% Fe_{py} (Fig. 10) in the LSI and the BIF. Equilibrium considerations indicate that pyrite formation in a dissolved Fe-rich water column will be controlled by the availability of sulfide rather than Fe. Sulfide was produced either at or near the sediment–water interface where organic matter was metabolized to drive the microbial reduction of dissolved sulfate to sulfide. C_{org} concentrations are high (2–4%) in both units, and there are no variations in the ratio C_{org}/Al (see Fig. 6) through the LSI and the BIF and thus it seems unlikely that C_{org} availability would limit sulfate reduction. However, sulfate was present at only low concentrations (probably $\ll 1$ mM; Canfield et al., 2000), so sulfate depletion was the most likely control on sulfide availability. As long as the basin contained some sulfate, depletion would not occur in surface sediments (where bottom waters would readily maintain the supply of sulfate) but would instead occur once sediments were buried beyond the depth where sulfate could be re-supplied by diffusion. Burial rates in turn depend on rates of clastic sediment delivery, and the uniform pyrite concentrations in the LSI and the BIF thus suggest that only relatively small changes in clastic sediment delivery rates occurred during their deposition. The changes in the Al contents of these units (see above) must therefore be mainly attributable to changes in the rates of hydrothermal Fe addition which affect the amounts of Fe precipitated as carbonate. Dilution

effects by carbonate operated through changes in the rates of hydrothermal Fe delivery that increased rates of siderite and ankerite precipitation to produce bulk sediments with low Al contents.

The uppermost part of ADBP-9 presents a contrasting picture of chemical conditions, notably in the high concentrations of pyrite in the upper shale interval (USI) which Reinhard et al. (2009) attributed to euxinic conditions in the water column. Values of Fe_T/Al remain relatively low throughout this part of the sequence (Fig. 4a). The highest Fe_T/Al values are found in the USI where euxinic conditions prevailed (Reinhard et al., 2009) reflecting the addition of authigenic Fe as pyrite (Fig. 6b) that exceeds Fe_{carb} and Fe_{sil} (Fig. 10). The increase in pyrite seems to have arisen from an increase in atmosphere oxygenation, which enhanced continental weathering of pyrite and thus delivery of dissolved sulfate. Increased sulfate delivery into the basin produced increased sulfate reduction and the sulfide was precipitated as pyrite (Reinhard et al., 2009). Increased atmospheric oxygenation would have allowed an iron shuttle to be established thus producing the pyrite spike in USI. However this spike may also be recorded because dissolved Fe was still available in the basin following earlier precipitation as carbonate and silicate. Enhanced concentrations of C_{org} in the USI (Fig. 6) are not associated with low Al contents and hence must be caused by increased productivity or preservation. We prefer to attribute these increases in C_{org} to increases in productivity which also facilitated the mid-water column euxinia, although we note that in some instances the sulfurization of relatively labile organic matter can improve organic carbon preservation in sulfidic environments (Sinninghe Damste et al., 1998; van Dongen et al., 2003).

The Fe chemistry of the uppermost carbonate C1 is unremarkable. Values of Fe_T/Al are relatively low and Fe is present mainly as Fe-rich dolomite or ankerite, with pyrite contents falling to pre-USI levels. This decrease in pyrite may indicate a return to low sulfate conditions in phase with lower atmospheric oxygen (Anbar et al., 2007; Kaufman et al., 2007)—perhaps through reaction with reduced crustal minerals (Reinhard et al., 2009). The precipitation of Fe-rich dolomite or ankerite rather than siderite probably indicates that dissolved Fe concentrations had fallen relative to dissolved Ca. It is reasonable to conclude that the weathering of pyrite on land would have produced more acidic surface waters capable of dissolving more carbonates, and thus the riverine delivery of dissolved Ca increased along with dissolved sulfate. The accumulation of dissolved Ca in the basin and the concomitant removal of Fe as pyrite ultimately produced seawater with molar activity ratios of $\{Fe^{2+}\}/\{Ca^{2+}\}$ below the levels needed to stabilize siderite (~ 0.05 ; Berner, 1971). Thus the primary authigenic phases became dolomite or ankerite.

The hypothesized changes in basin chemistry are shown schematically in Fig. 11. The first significant control is the relative concentrations of dissolved Fe and sulfide. The right-hand pathway shows that sulfide-dominated waters produce iron-limited conditions that are recorded by pyritic sediments with high DOP values (>0.8) and high Fe_{HR}/Fe_T

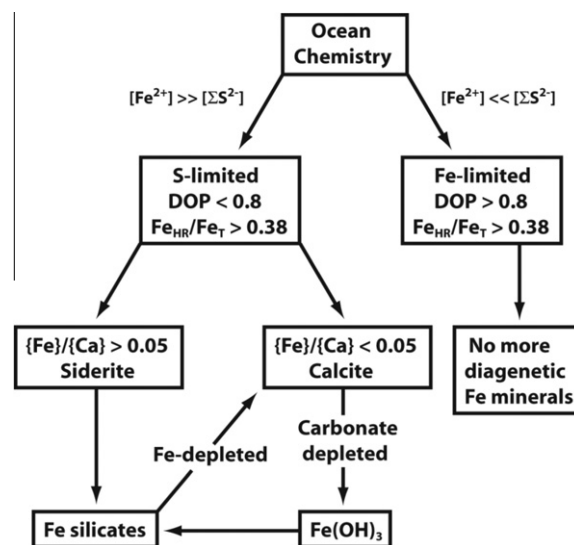


Fig. 11. Schematic pathway showing chemical controls on authigenic mineral formation in the Mt. McRae Shale.

(>0.38). These conditions produced no additional, Fe-bearing diagenetic minerals because the presence of dissolved sulfide maintains dissolved Fe at levels that are too low to stabilize iron carbonates or silicates (see earlier). The left-hand pathway in Fig. 11 is more complex. High concentrations of dissolved Fe relative to dissolved sulfide produce anoxic (but not euxinic) waters, yielding sediments with low pyrite contents and $DOP < 0.8$ and $Fe_{HR}/Fe_T > 0.38$ (Reinhard et al., 2009). The next significant control operates through the molar $\{Fe^{2+}\}/\{Ca^{2+}\}$ activity ratio. Berner (1971) showed that values >0.05 enable siderite formation (which we have found to be associated with Fe-rich silicate formation) and values <0.05 stabilize only Fe-poor carbonates (such as calcite) or Fe-poor silicates. The final control reflects the balance between dissolved Fe and dissolved carbonate. Dissolved Fe in excess of dissolved carbonate would allow continued formation of Fe-rich silicates possibly accompanied by $Fe(OH)_3$, but an excess of dissolved carbonate after the depletion of dissolved Fe would only allow calcite and/or dolomite to precipitate. The relative importance of the various pathways is determined not only by rates of cation and anion supply relative to rates of removal but also by rates of sediment accumulation that may act to limit these supplies by limiting the exposure time (and hence the reaction time) for syngenetic or early diagenetic mineral precipitation prior to burial. Our work re-asserts the value of iron speciation approaches in unraveling complex depositional and diagenetic patterns in Precambrian rocks while emphasizing the need for case-by-case method validation accompanied by detailed mineralogy. This approach to iron speciation shows how mineralogy is controlled by the variable interplay atmospheric oxygen levels and oceanic chemistry, the latter in turn controlled by sources of iron to the deep basin, sulfide sourced by sulfate reduction, and rates of clastic sedimentation.

ACKNOWLEDGMENTS

Funding was provided to T.W.L. and A.A. by the NASA Exobiology Program and Astrobiology Institute and the Geobiology and Low-Temperature Geochemistry Program of the NSF. Ben Gill helpfully provided most of the euxinic data in Fig. 5. Dave Johnston and one anonymous reviewer are thanked for their comments, as is Bob Aller for his thorough editorial assistance.

APPENDIX A. SUPPLEMENTARY DATA

Supplementary data associated with this article can be found, in the online version, at doi:10.1016/j.gca.2010.11.013.

REFERENCES

- Alibert C. and McCulloch M. T. (1993) Rare earth element and neodymium isotope compositions of the banded iron formations and associated shales from the Hamersley, Western Australia. *Geochim. Cosmochim. Acta* **57**, 187–204.
- Anbar A. D., Duan Y., Lyons T. W., Arnold G. L., Kendall B., Creaser R. A., Kaufman A. J., Gordon G. W., Scott C., Garvin J. and Buick R. (2007) A whiff of oxygen before the Great Oxidation Event? *Science* **317**, 1903–1906.
- Bau M. and Moller P. (1993) Rare earth element systematic of the chemically-precipitated component in Early Precambrian iron formations and the evolution of the terrestrial atmosphere–hydrosphere–lithosphere system. *Geochim. Cosmochim. Acta* **57**, 2239–2249.
- Bekker A., Holland H. D., Wang P.-L., Rumble, III, D., Stein H. J., Hannah J. L., Coetzee L. L. and Beukes N. J. (2004) Dating the rise of atmospheric oxygen. *Nature* **427**, 117–120.
- Berner R. A. (1971) *Principles of Chemical Sedimentology*. McGraw-Hill, New York.
- Brigattini M. F., Galan E. and Theng B. K. G. (2006) Structures and mineralogy of clay minerals. In *Handbook of Clay Science* (eds. F. Bergaya, B. K. G. Theng and G. Lagaly). Amsterdam, Elsevier, pp. 19–86.
- Canfield D. E. (2005) The early history of atmospheric oxygen. *Annu. Rev. Earth Planet. Sci.* **33**, 1–36.
- Canfield D. E. and Raiswell R. (1991) Carbonate precipitation and dissolution: its relevance to fossil preservation. In *Taphonomy: Releasing the Data Locked in the Fossil Record* (eds. P. A. Allison and D. E. G. Briggs). Plenum, New York, pp. 412–453.
- Canfield D. E., Lyons T. W. and Raiswell R. (1996) A model for iron deposition to euxinic Black Sea sediments. *Am. J. Sci.* **296**, 818–834.
- Canfield D. E., Habicht K. S. and Thamdrup B. (2000) The Archean sulfur cycle and the early history of atmospheric oxygen. *Science* **288**, 658–661.
- Canfield D. E., Raiswell R., Westrich J. T., Reeves C. M. and Berner R. A. (1986) The use of chromium reduction in the analysis of reduced inorganic sulphur in sediments and shales. *Chem. Geol.* **54**, 149–155.
- Clarke F. W. (1924) *Data on Geochemistry*. US Geological Survey Bulletin 770.
- Cornell R. M. and Schwertmann U. (2003) *The Iron Oxides: Structure, Properties, Reactions, Occurrences and Uses*. Wiley, New York.
- Cruse A. M. and Lyons T. W. (2004) Trace metal records of regional paleoenvironmental variability in Pennsylvanian (Upper Carboniferous) black shales. *Chem. Geol.* **206**, 319–345.
- Derry L. A. and Jacobsen S. B. (1990) The chemical evolution of Precambrian seawater: evidence from REEs in banded iron formations. *Geochim. Cosmochim. Acta* **54**, 2965–2977.
- Ewers W. C. and Morris R. C. (1981) Studies of the Dales Gorge Member of the Brockman Iron formation, Western Australia. *Econ. Geol.* **76**, 1929–1953.
- Fischer W. W. and Knoll A. H. (2009) An iron shuttle for deepwater silica in Late Archean and early Proterozoic iron formation. *Bull. Geol. Soc. Am.* **121**, 222–235.
- Gill B. C. (2009) High-resolution sulfur isotope records of the Paleozoic and a detailed geochemical study of the late Cambrian SPICE event utilizing sulfur isotope stratigraphy, metal chemistry and numerical modeling. Unpublished Ph.D., University of California, Riverside.
- Gole M. J. (1980) Mineralogy and petrology of very-low-metamorphic grade Archean banded iron-formations, Weld Range, Western Australia. *Am. Mineral.* **65**, 8–25.
- Gole M. J. (1981) Archean banded iron-formations, Yilgarn Block, Western Australia. *Econ. Geol.* **78**, 1954–1974.
- Grotzinger J. P. and Kasting J. F. (1993) New constraints on Precambrian ocean chemistry. *J. Geol.* **101**, 235–243.
- Hatch J. R. and Leventhal J. S. (1992) Relationship between inferred redox potential of the depositional environment and geochemistry of the Upper Pennsylvanian (Missourian) Stark Shale Member of the Dennis limestone, Wabaunsee County, Kansas, U.S.A.. *Chem. Geol.* **99**, 65–82.
- Holland H. D. (1962) Model for the evolution of the Earth's atmosphere. In *Petrologic Studies: A Volume in Honor of A.F. Buddington* (eds. A. E. J. Engel, H. L. James and B. F. Leonard). *Geol. Soc. Am.*, Boulder, Colorado, pp. 447–477.
- Holland H. D. (1984) *The Chemical Evolution of the Atmosphere and Oceans*. Wiley-Interscience, New York, 351p.
- Holland H. D. (1992). In *The Proterozoic Biosphere* (eds. J. W. Schopf and C. Klein). Cambridge University Press, pp. 153–155.
- Holland H. D. (2002) Volcanic gases, black smokers and the great oxidation event. *Geochim. Cosmochim. Acta* **66**, 3811–3826.
- Kakegawa T., Kawal H. and Ohmoto H. (1999) Origins of pyrite in the 2.5 Ga Mt. McRae Shale, The Hamersley District, Western Australia. *Geochim. Cosmochim. Acta* **62**, 3205–3220.
- Kendall B., Reinhard C. T., Lyons T. W., Kaufman A. J., Poulton S. W. and Anbar A. (2010) Pervasive oxygenation along Late Archean ocean margins. *Nat. Geosci.* **3**, 647–652.
- Karhu J. A. and Holland H. D. (1994) Carbon isotopes and the rise in atmospheric oxygen. *Geology* **24**, 867–870.
- Kaufman A. J., Johnston D. T., Farquhar J., Masterson A. L., Lyons T. W., Bates S., Anbar A. D., Arnold G. L., Garvin J. and Buick R. (2007) Late Archean biospheric oxygenation and atmospheric evolution. *Science* **317**, 1900–1906.
- Klein C. (2005) Some Precambrian banded iron formations (BIFs) from around the world: their age. Geologic setting, mineralogy, metamorphism, geochemistry, and origin. *Am. Mineral.* **90**, 1473–1499.
- Klein C. and Bricker O. P. (1977) Some aspects of the sedimentary and diagenetic environment of Proterozoic banded iron-formation. *Econ. Geol.* **72**, 1457–1470.
- Klein C. and Beukes N. J. (1989) Geochemistry and sedimentology of a facies transition from limestone to iron-formation deposition in the Early Proterozoic Transvaal supergroup, South Africa. *Econ. Geol.* **84**, 1733–1774.
- Krapez B., Barley M. E. and Pickard A. I. (2003) Hydrothermal and resedimented origins of the precursor sediments to banded iron formation: sedimentological evidence from the Early Precambrian Brockman Supersequence of Western Australia. *Sedimentology* **50**, 970–1011.

- Kump L. R. and Holland H. D. (1992) Iron in Precambrian rocks: implications for the global oxygen budget of the ancient earth. *Geochim. Cosmochim. Acta* **56**, 3217–3223.
- LaBerge G. L. (1966) Altered pyroclastic rocks in iron-formation in the Hamersley Range, Western Australia. *Econ. Geol.* **61**, 147–161.
- LaBerge G. L., Robbins E. I. and Han T.-M. (1987) A model for the biological precipitation of Precambrian iron-formations-A: geological evidence. In *Precambrian Iron Formation* (eds. P. W. U. Appel and G. L. LaBerge). Theophrastus, Athens, pp. 69–97.
- Lyons T. W. and Severmann S. (2006) A critical look at iron paleoredox proxies based on new insights from modern euxinic marine basins. *Geochim. Cosmochim. Acta* **70**, 5698–5722.
- Maynard J. (1983) *Geochemistry of Sedimentary Ore Deposits*. Springer-Verlag, New York, 305p.
- McConchie D. (1987) The geology and geochemistry of the Joffre and Whaleback Shale members of the Brockman Iron Formation, Western Australia. In *Precambrian Iron Formation* (eds. P. W. U. Appel and G. L. LaBerge). Theophrastus, Athens, pp. 541–597.
- Millero F. J. (2001) *The Physical Chemistry of Natural Waters*. Wiley-Interscience, New York, 654p.
- Mongenot T., Tribouillard N.-P., Desprairies A., Lallier-Vergas E. and Laggoun-Defarge F. (1996) Trace elements as paleoenvironmental markers in strongly mature hydrocarbon source rocks: the Cretaceous La Luna Formation of Venezuela. *Sediment. Geol.* **103**, 23–37.
- Morris R. C. (1993) Genetic modeling for banded iron-formation of the Hamersley Group, Pilbara Craton, Western Australia. *Precambrian Res.* **60**, 243–286.
- Morris R. C. and Horowitz R. C. (1983) The origin of the iron-formation-rich Hamersley Group of Western Australia—deposition on a platform. *Precambrian Res.* **21**, 273–297.
- Ohmoto H., Watanabe Y. and Kumazawa K. (2004) Evidence from massive siderite beds for a CO₂-rich atmosphere before 1 ~ 1.8 billion years ago. *Nature* **429**, 395–399.
- Ohmoto H., Watanabe Y., Yamaguchi K. E., Naraoka H., Haruna M., Kakegawa T., Hayashi K. and Kato Y. (2006) Chemical and biological evolution of early earth: constraints from banded iron formations. In *Evolution of the Earth's Early Atmosphere, Hydrosphere and Biosphere—Constraints from Ore Deposits*, vol. 198 (eds. S. E. Kesler and H. Ohmoto). *Geol. Soc. Am. Memoir*, pp. 291–331.
- Omotoso O., McCarty D. K., Hiller S. and Kleeberg R. (2006) Some successful approaches to quantitative mineral analysis as revealed by the 3rd Reynolds Cup contest. *Clays Clay Miner.* **54**, 751–763.
- Ono S., Eigenbrode J. L., Pavlov A. A., Karecha P., Rumble, III, D., Kasting J. F. and Freeman K. H. (2003) New insights into Archean sulfur cycle from mass-independent sulfur isotope records from the Hamersley Basin, Australia. *Earth Planet. Sci. Lett.* **213**, 15–30.
- Pecoits E., Gingras M. K., Barley M. E., Kappler A., Posth N. R. and Konhauser K. (2009) Petrography and geochemistry of the Dales Gorge banded iron formation: paragenetic sequence, source and implications for paleo-ocean chemistry. *Precambrian Res.* **172**, 163–187.
- Pickard A. P., Barley M. E. and Krapez B. (2004) Deep-marine depositional setting of banded iron formation: sedimentological evidence from interbedded clastic sedimentary rocks in the early Paleoproterozoic Dales Gorge Member of Western Australia. *Sediment. Geol.* **170**, 37–62.
- Poulton S. W., Fralick P. W. and Canfield D. E. (2004) The transition to a sulphidic ocean ~1.84 billion years ago. *Nature* **431**, 173–177.
- Poulton S. W. and Canfield D. E. (2005) Development of a sequential extraction procedure for iron: implications for iron partitioning in continentally derived particulates. *Chem. Geol.* **214**, 209–221.
- Raiswell R. (2006) An evaluation of diagenetic recycling as a source of iron for banded iron formations. In *Evolution of the Earth's Early Atmosphere, Hydrosphere and Biosphere—Constraints from Ore Deposits*, vol. 198 (eds. S. E. Kesler and H. Ohmoto). *Geol. Soc. Am. Memoir*, pp. 223–238.
- Raiswell R. and Canfield D. E. (1998) Sources of iron for pyrite formation. *Am. J. Sci.* **298**, 219–245.
- Raiswell R. and Anderson T. F. (2005) Reactive iron enrichment in sediments deposited beneath euxinic bottom waters: constraints on supply by shelf recycling. In *Mineral Deposits and Earth Evolution*, vol. 248 (eds. I. McDonald, A. Boyce, I. B. Butler, R. J. Herrington and D. Poly). *Geol. Soc. Lond. Spec. Publ.*, pp. 179–194.
- Raiswell R., Buckley F., Berner R. A. and Anderson T. F. (1988) Degree of pyritization of iron as a paleoenvironmental indicator. *J. Sediment. Petrol.* **58**, 812–819.
- Raiswell R., Canfield D. E. and Berner R. A. (1994) A comparison of iron extraction methods for the determination of degree of pyritisation and the recognition of iron-limited pyrite formation. *Chem. Geol.* **111**, 101–111.
- Raiswell R., Newton R., Bottrell S. H., Coburn P., Briggs D. E. G., Bond D. P. G. and Poulton S. W. (2008) Turbidite depositional influences on the diagenesis of Beecher's Trilobite Bed and the Hunsrück Slates: sites of soft tissue preservation. *Am. J. Sci.* **308**, 105–129.
- Reinhard C. T., Raiswell R., Scott C., Anbar A. D. and Lyons T. W. (2009) A late Archean sulfidic sea stimulated by early oxidative weathering of the continents. *Science* **326**, 713–716.
- Rickard D. and Luther G. W. I. I. (2007) Chemistry of iron sulfides. *Chem. Rev.* **107**, 514–562.
- Ronov A. B. and Migdisov A. A. (1971) Geochemical history of crystalline basement and sedimentary cover of the Russian and North American Platforms. *Sedimentology* **16**, 173–183.
- Rye R., Kuo P. H. and Holland H. D. (1995) Atmospheric carbon dioxide concentrations before 2.2 billion years ago. *Nature* **378**, 603–605.
- Severmann S., Lyons T. W., Anbar A., McManus J. and Gordon G. (2008) Modern iron isotope perspectives on the benthic iron shuttle and the redox evolution of ancient oceans. *Geology* **36**, 487–490.
- Shen Y., Knoll A. H. and Walter M. R. (2003) Evidence for low sulphate and anoxia in a mid-Proterozoic marine basin. *Nature* **423**, 632–635.
- Sinninghe Damste J. S., Kok M. D., Koster J. and Schouten S. (1998) Sulfurized carbohydrates: an important sedimentary sink for organic carbon? *Earth Planet. Sci. Lett.* **164**, 7–13.
- Srodon J., Drits V. A., McCarty D. K., Hsieh J. C. C. and Eberl D. D. (2001) Quantitative XRD analysis of clay-rich rocks from random preparations. *Clays Clay Miner.* **49**, 514–528.
- Stookey L. L. (1970) Ferrozine—a new spectrophotometric reagent for iron. *Anal. Chem.* **42**, 779–781.
- Tardy Y. and Garrels R. M. (1974) A method of estimating the Gibbs energies of formation of layer silicates. *Geochim. Cosmochim. Acta* **38**, 1101–1116.
- Taylor S. R. and McLennan S. M. (1985) *The Continental Crust: Its Composition and Evolution*. Blackwell, Oxford University Press.
- Trendall A. F. and Blockley J. G. (1970) The iron formations of the Precambrian Hamersley Group, Western Australia: with special reference to the associated crocidolite. *West. Aust. Geol. Surv. Bull.* **119**, 336.

- Tribovillard N.-P., Desprairies A., Lallier-Vergas E., Bertrand P., Moureau N., Ramdani A. and Ramanampisoa L. (1993) Geochemical study of organic-matter rich cycles from the Kimmeridge Clay Formation of Yorkshire (UK): productivity versus anoxia. *Paleogeogr. Paleoclimatol. Paleoecol.* **108**, 165–181.
- van Dongen B. E., Schouten S., Bass M., Geenevasen A. J. and Sinninghe Damste J. S. (2003) An experimental study of the low-temperature sulfurization of carbohydrates. *Org. Geochem.* **34**, 1129–1144.
- Velde B. (2003) Green clay minerals. In *Treatise on Geochemistry*, 7.12. Elsevier, Amsterdam, pp. 309–324.
- Waite T. D. (2001) Thermodynamics of the iron system in seawater. In *The Biogeochemistry of Iron in Seawater* (eds. D. R. Turner and K. A. Hunter). Wiley, New York, pp. 291–339.
- Walker J. C. G. (1983) Possible limits on the composition of the Archean ocean. *Nature* **302**, 518–520.
- Webb A. D., Dickens G. R. and Oliver N. H. S. (2003) From banded iron-formation to iron ore: geochemical and mineralogical constraints from across the Hamersley Province, Western Australia. *Chem. Geol.* **197**, 215–252.
- Werne J., Sageman B. B., Lyons T. W. and Hollander D. J. (2002) An integrated assessment of a ‘type euxinic’ deposit: evidence for multiple controls on black shale deposition in the Middle Devonian Oatka Creek Formation. *Am. J. Sci.* **302**, 110–143.
- Woods T. L. and Garrels R. M. (1987) *Thermodynamic Values at Low Temperature for Natural Inorganic Materials: An Uncritical Summary*. Oxford University Press, 242p.

Associate editor: Robert C. Aller